NANO LETTERS
Letter
Cite This: Nano Lett. 2018, 18, 2590−2594
pubs.acs.org/NanoLett

Probing Phonon Dynamics in Individual Single-Walled Carbon Nanotubes

Tao Jiang,[†] Hao Hong,[‡] Can Liu,[‡] Wei-Tao Liu,[†,§] Kaihui Liu,[*,‡] and Shiwei Wu[*,†,§]

[†]State Key Laboratory of Surface Physics, Key Laboratory of Micro and Nano Photonic Structures, and Department of Physics, Fudan University, Shanghai 200433, China

[‡]State Key Laboratory for Mesoscopic Physics, Collaborative Innovation Center of Quantum Matter, and School of Physics, Peking University, Beijing 100871, China

[§]Collaborative Innovation Center of Advanced Microstructures, Nanjing 210093, China

S *Supporting Information*

ABSTRACT: Interactions between elementary excitations, such as carriers, phonons, and plasmons, are critical for understanding the optical and electronic properties of materials. The significance of these interactions is more prominent in low-dimensional materials and can dominate their physical properties due to the enhanced interactions between these excitations. One-dimensional single-walled carbon nanotubes provide an ideal system for studying such interactions due to their perfect physical structures and rich electronic properties. Here we investigated G-mode phonon dynamics in individual suspended chirality-resolved single-walled carbon nanotubes by time-resolved anti-Stokes Raman spectroscopy. The improved technique allowed us to probe the intrinsic phonon information on a single-tube level and exclude the influences of tube−tube and tube−substrate interactions. We found that the G-mode phonon lifetime ranges from 0.75−2.25 ps and critically depends on whether the tube is metallic or semiconducting. In comparison with the phonon lifetimes in graphene and graphite, we revealed structure-dependent carrier−phonon and phonon−phonon interactions in nanotubes. Our results provide new information for optimizing the design of nanotube electronic/optoelectronic devices by better understanding and utilizing their phonon decay channels.

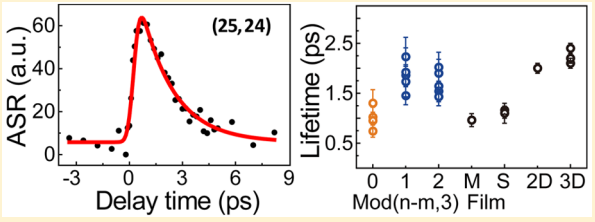

KEYWORDS: *Single-walled carbon nanotubes, phonon dynamics, time-resolved anti-Stokes Raman spectroscopy, chirality, carrier−phonon coupling, phonon−phonon interaction*

Ever since the discovery of single-walled carbon nanotubes (SWNTs),[1] their plentiful physical properties that are uniquely determined by the chiral indices (n,m) or chirality have attracted tremendous scientific and technological interests. In such a one-dimensional (1D) system, enhanced interactions between elementary excitations such as carriers, phonons, and plasmons, play an important role in determining their physical properties.[2−5] Among these interactions, phonon scattering is one very important aspect, which dominates not only the Raman spectra, but also other physical properties such as electrical and thermal conductivity. For example, carrier−phonon coupling leads to current saturation in high-field ballistic transport,[6−8] and phonon−phonon coupling provides anharmonic decay channel for optical phonons and affects thermal conductivity.[8−12] These phonon dynamics have been studied by the line width of corresponding Raman mode, which provides an indirect (and inaccurate) method to reveal phonon lifetime.[13,14] Meanwhile, femtosecond pump−probe techniques are known to probe the dynamics in time domain.[15] Indeed, many pump−probe studies have been done on carbon nanotubes in the past, and even a few reports were done at a single-tube level.[16−18] Yet, most of these pump−probe studies were based on transient absorption spectroscopy, in which the phonon lifetime is indirectly deduced from carrier dynamics and many different phonons could contribute to the relaxation of excited carriers. Recently, time-resolved anti-Stokes Raman (ASR) spectroscopy was developed to directly probe the dynamics of zone-center optical phonons in two-dimensional (2D) graphene or nanotube films by using the ASR intensity to monitor the time evolution of phonon population.[11,12,19−23] However, at a single-tube level, due to the extremely small anti-Stocks Raman scattering signal, the detection of phonon dynamics of individual nanotubes with defined chirality is still of great challenge.

Here we revealed the first chirality-dependent phonon lifetime of individual suspended SWNTs by time-resolved anti-Stokes Raman spectroscopy so that tube-substrate and tube−tube interactions could be excluded. Furthermore, we found that the phonon lifetime decays faster in metallic SWNTs than that in semiconducting SWNTs because the carrier−phonon coupling via Landau damping acts as additional

Received: January 24, 2018
Revised: February 21, 2018
Published: March 15, 2018

DOI: 10.1021/acs.nanolett.8b00341
Nano Lett. 2018, 18, 2590−2594

phonon relaxation channel in metallic tubes. In comparison with the previous results from 2D graphene and 3D graphite,[21−23] the role of dimensionality in affecting phonon relaxation is also discussed. These findings would not be possible without a direct measurement on chirality-resolved suspended SWNTs. Our experimental results would also stimulate detailed theoretical understanding of energy dissipation in low-dimensional graphitic materials and further foster the technological developments based on individual SWNTs.

In our studies, all suspended SWNTs were grown across an open slit fabricated on silicon substrates by chemical vapor deposition (CVD) with the method described in the Supporting Information. The SWNTs were sparsely distributed such that there is only one tube within diffraction limited laser focal spots. This sample geometry, schematically shown in Figure 1a, enables the possibility for electron diffraction in transmission electron microscope (TEM) and optical spectroscopy without the influence of scattering background from neighboring tubes and extrinsic effects from the substrate. Therefore, the chiral index of each SWNT can be identified precisely by both TEM electron diffraction[24−26] and optical spectroscopy.[27−30] Figure 1b−d show the results of one representative SWNT. The chiral index of this SWNT was determined to be (28,7) from the electron diffraction pattern (Figure 1b), indicating that it is a metallic tube with a diameter of 2.51 nm. The corresponding Rayleigh scattering (Figure 1c) and absorption spectra (Figure 1d) revealed two optical resonances at 2.01 and 2.28 eV in energy range of 1.50−2.60 eV, corresponding to M_{22}^{-} and M_{22}^{+} transitions of this SWNT.

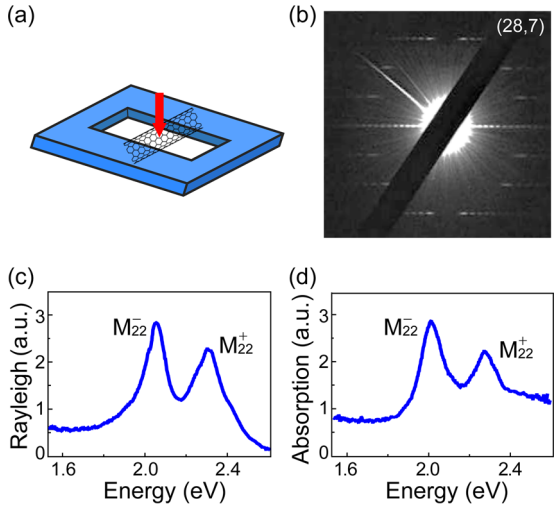

Figure 1. Electron diffraction pattern and optical spectra of a suspended SWNT. (a) Schematic of suspended nanotube sample for both electron diffraction and optical measurements. (b) Electron diffraction pattern indicates the chirality of this SWNT to be (28,7), a metallic tube with diameter of 2.51 nm. (c) Rayleigh and (d) absorption spectra of (28,7) SWNT, respectively. The two resonances at 2.01 and 2.28 eV correspond to the M_{22}^{-} and M_{22}^{+} electronic transitions, respectively.

Time-resolved ASR spectroscopy is a direct method to measure the phonon lifetime of materials in time domain. The phonon populations can be directly traced out by recording the ASR intensity under different time delay between the near-infrared pump and visible probe laser beams.[11,12,15,19−23] Compared to 2D graphene, 1D SWNT has on average three orders of magnitude smaller ASR signal (due to 1D ≈ 1 nm nanotube diameter in a 2D ≈ 1 μm diameter laser focus), making the measurement more challenging. Here in our experiment, since we have already known the electronic structure of every nanotube, we can purposely choose the photon energy of the probe beam to match the nanotube optical resonance, which greatly enhanced the very weak ASR intensity by orders of magnitude and made the single-tube level signal detectable. Meanwhile, the wavelength of the pump beam was fixed at 820 nm, which is longer than that of the probe beam. In addition, our time-resolved ASR spectroscopic measurements were performed under a home-built optical microscopic setup (see Supporting Information, Figure S2). The pump and probe beams were sent collinearly through a microscopic objective (Nikon, 50X/NA0.45) onto the individual SWNTs. The laser polarizations were parallel to the SWNT axis to obtain stronger excitation and detection signal. The emitted ASR signal in the backscattered direction was collected by the same objective and analyzed by a liquid nitrogen cooled silicon CCD detector after passing through a spectrograph with appropriate filters.

We first examined the ASR spectra at different time delays. Figure 2a displays the selected ASR spectra of G-mode phonons at ∼1585 cm^{-1} for a semiconducting (25,24) SWNT acquired at five different time delays. At time delay of −3.4 ps (the probe pulse ahead the pump pulse), the ASR peak was very weak. However, when the probe pulse arrived after the pump pulse, the ASR peak intensity became higher and evolved with time delay indicating obvious phonon dynamics. To quantitatively see how the phonon population of the G-mode evolves with time, we monitored the G-mode phonon dynamics by varying the time delay and recording the corresponding ASR

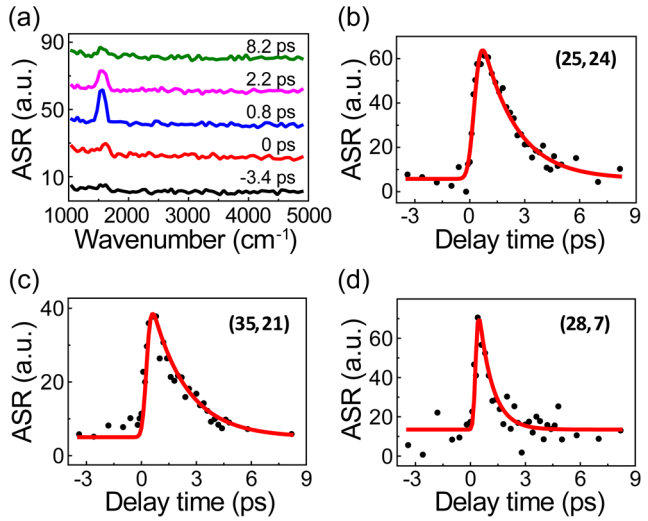

Figure 2. Phonon dynamics of individual SWNTs with defined chirality. (a) Anti-Stokes Raman (ASR) spectra at different time delays between pump and probe pulses measured from a (25,24) SWNT. While the pump beam was fixed at 820 nm, the probe beam was purposely tuned to the photon energy that matches with the nanotube optical resonance. In the case of (25,24) SWNT, the photon energy of the probe beam was 1.95 eV. The exposure time for each spectrum was 1 min. (b−d) Integrated intensity of G-mode ASR peak at ∼1585 cm^{-1} plotted as a function of time delay for three representative SWNTs with different chiralities of (b) (25,24), (c) (35,21), and (d) (28,7), respectively. The fitted lifetimes are 1.86 ± 0.21, 1.90 ± 0.28, and 0.74 ± 0.12 ps, respectively.

DOI: 10.1021/acs.nanolett.8b00341
Nano Lett. 2018, 18, 2590−2594

intensity. The integrated intensity of the ASR peaks was extracted from the spectra and plotted as a function of time delay. Figure 2b depicts the time-resolved ASR integrated peak intensity of the same semiconducting (25,24) SWNT as in Figure 2a. The ASR peak intensity, which is proportional to the phonon population, was very weak before time-zero but reached the maximum after several hundred femtoseconds, then decayed away to a lowest constant value in the next few picoseconds. The nonzero constant ASR intensity is attributed to a weak, time-independent background from hot phonons created by the probe beam.

For comparison with semiconducting (25,24) SWNT with mod(n−m,3) = 1, the phonon dynamics of a semiconducting (35,21) SWNT with mod(n−m,3) = 2 and a metallic (28,7) SWNT with mod(n−m,3) = 0 are also presented in Figure 2c and d, respectively. All of these three types of nanotubes showed similar phonon dynamic behavior except the decay time. We reproduced the dynamic results by convoluting the finite pulse duration with intrinsic phonon dynamics in SWNT, with the details described in the Supporting Information and ref 23. G-mode phonon lifetime was also determined by fitting the relaxation section with a single exponential decay. The lifetimes were found to be 1.86 ± 0.21, 1.90 ± 0.28, and 0.74 ± 0.12 ps for the semiconducting (25,24), (35,21), and metallic (28,7) SWNT, respectively. According to these values, the phonon lifetimes of the two semiconducting SWNTs are very close to each other although these two SWNTs have different chiralities and mod(n−m,3) values. However, the phonon lifetime of the metallic SWNT is much smaller than that of the two semiconducting SWNTs.

To have more statistic information, we conducted time-resolved ASR spectroscopy measurements on 14 SWNTs in total (summarized in Table S1 in Supporting Information). Figure 3a displays the phonon lifetime statistics of all these

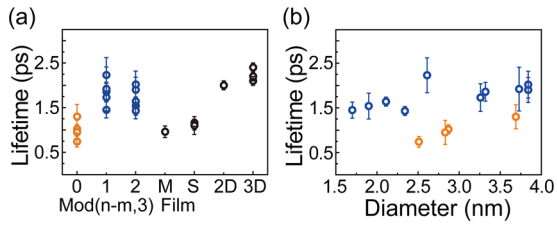

Figure 3. Phonon lifetime statistics of 14 SWNTs and the other two graphitic materials (2D graphene and 3D graphite). (a) Phonon lifetimes of SWNTs are shown by classifying mod(n−m,3) values. The metallic SWNTs with mod(n−m,3) = 0 show phonon lifetime ∼1.0 ps, while the semiconducting SWNTs with mod(n−m,3) = 1 or 2 show phonon lifetime ∼1.75 ps. For comparison, the phonon lifetimes of metallic (M) and semiconducting (S) SWNTs films (0.9−1.2 ps),[11,19,20] suspended monolayer graphene (2.0 ps)[23] and graphite (2.2 ps),[21−23] are also plotted. (b) Phonon lifetime as a function of nanotube diameter. Blue and orange circles correspond to semiconducting and metallic SWNTs, respectively. The phonon lifetime increases correspondingly with diameter enlarging and exhibits larger increase rate in metallic SWNTs than in semiconducting ones.

SWNTs. We also plotted the phonon lifetimes of metallic/semiconducting SWNTs films,[11,19,20] suspended 2D graphene,[23] and 3D graphite[21−23] for comparison. To investigate the difference of phonon lifetime between semiconducting and metallic SWNTs, the phonon lifetimes of SWNTs are classified by mod(n−m,3) values. For mod(n−m,3) = 0, all of the four metallic SWNTs show phonon lifetimes shorter than 1.4 ps, while for mod(n−m,3) = 1 or 2, the semiconducting SWNTs show phonon lifetimes longer than 1.4 ps. The statistic result shows no obvious trend differences of phonon lifetimes between the two kinds semiconducting SWNTs with mod(n−m,3) = 1 or 2. However, metallic SWNTs have shorter phonon lifetimes (∼1.0 ps) than that of semiconducting SWNTs (∼1.75 ps). In addition, the phonon lifetimes of suspended monolayer graphene (∼2.0 ps) and graphite (∼2.2 ps) are longer than the average value of metallic SWNTs. We also plotted the phonon lifetime as a function of tube diameter in Figure 3b. For both semiconducting and metallic SWNTs, the phonon lifetime increases with tube diameter in the range of 1.5−4.0 nm. Furthermore, the phonon lifetime increases much faster in metallic SWNTs when the tube diameter enlarges. In addition, we also found that when the chiral angle increases, the phonon lifetime increases correspondingly in metallic SWNTs, while it remains constant in semiconducting ones (Figure S1 in Supporting Information).

To understand these nontrivial phonon dynamics differences, the electronic band structure of graphene and SWNTs are shown in Figure 4. The band structure of SWNTs can be

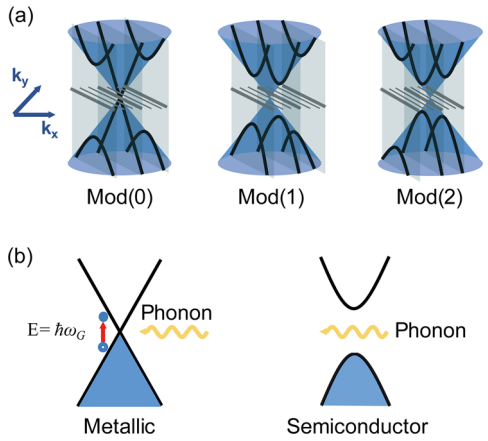

Figure 4. Electronic structures of graphene and SWNTs. (a) Diagram of zone-folding method. Band structure of SWNT is composed of curves from series of cutting lines (gray lines) on that of graphene. Considering the positions of cutting lines, SWNT can be classified by the value of mod(n−m,3). Mod(0) corresponds to metallic SWNT, while the other two are semiconducting SWNT. (b) Illustration of Landau damping in metallic SWNTs. Low energy carriers in a form of electron−hole pairs can be excited by absorbing G-mode phonons. This coupling mechanism forms an equilibrated phonon−carrier system, effectively expediting the G-mode phonon relaxation in metallic SWNTs, while the Landau damping is forbidden in semiconducting SWNTs due to their large electronic bandgap (>0.5 eV).

simply derived from that of graphene by zone-folding method,[31] as shown in Figure 4a. Different periodic boundary condition along the circumferential direction of SWNTs determines the different position of cutting lines. If the cutting line passes through the Dirac point of graphene, SWNT shows a zero band gap in the 1D band structure and becomes a metallic tube. Otherwise, SWNT is semiconducting. Figure 4b shows the band structure difference between metallic and semiconducting SWNTs.

We first discuss why the G-mode phonons decay faster in 1D metallic SWNTs than 2D graphene and 3D graphite. Phonon−phonon interaction and carrier−phonon coupling are two main

DOI: 10.1021/acs.nanolett.8b00341
Nano Lett. 2018, 18, 2590−2594

channels for phonon relaxation in graphitic materials. In nanotube system, phonon−phonon interaction is much stronger than that in graphene or graphite system because momentum matching for anharmonic phonon coupling is generally relaxed in 1D system. Specifically, zone-center G-mode optical phonons strongly couple to the unique 1D low-frequency mode phonons such as the radial breathing, pinch, bending modes, and long-wavelength acoustic phonons in carbon nanotube.[12,32] In addition, the carrier−phonon coupling in 1D system is generally stronger than 2D or 3D system due to the reduced dimensionality and stronger localization of excitonic wave function.[33−36] Therefore, phonons in metallic nanotubes decay faster than graphene or graphite.

Then we elucidate why the G-mode phonons decay faster in metallic SWNTs than semiconducting ones. The strength of phonon−phonon interaction is almost the same for these two kinds of tubes, while the carrier−phonon coupling is much different. In metallic SWNTs, the coupling between low energy carriers and acoustic phonons is largely enhanced, and they become an equilibrated system after the first few hundred femtoseconds.[23] G-mode phonons not only could decay into acoustic phonons via anharmonic coupling, but also could interact strongly with low energy carriers via Landau damping[37] (schematically shown in Figure 4b). Thus, the coupled system between low energy carriers and acoustic phonons expedites the relaxation of G-mode optical phonons. In contrast, the carrier−phonon coupling via Landau damping is forbidden in semiconducting SWNTs because the small energy of G-mode phonons (∼0.2 eV) is unable to generate electron−hole pairs in a large bandgap (typically >0.5 eV in our nanotubes). Thus, the carrier−phonon coupling in semiconducting SWNTs is much weaker than that in metallic ones, which results in shorter phonon lifetime in metallic SWNTs.

At last, we explicate the mechanism of diameter-dependent phonon lifetime in SWNTs. When the diameter enlarges, both nanotube curvature and phonon−phonon coupling strength reduce, giving rise to an increase of phonon lifetime. For metallic SWNTs, soften quantum confinement in larger diameter nanotube leads to even weaker electron−phonon coupling, accounting for more rapid lifetime increment. This is consistent with the line width narrowing of G-mode Raman peak in metallic SWNTs for larger tube diameter.[13,14]

Now knowing the phonon dynamics of individual SWNTs with defined chirality, it would be interesting to compare the phonon lifetime with ensemble measurements. Song et al. measured on a thin film of SWNTs that was predominantly of (6,5) semiconducting tubes, and the G-mode phonon lifetime was determined to be 1.1 ± 0.2 ps.[11] Similar measurements were done on thin films of semiconducting and metallic SWNTs by Kang et al.,[19] and the phonon lifetimes were found to be 1.2 and 0.9 ps, respectively. The measured values on the ensemble of SWNTs are noticeably shorter than that of an isolated and suspended single semiconducting SWNT (∼1.75 ps) and almost resemble that of individual metallic SWNT (∼1.0 ps). This fact suggests that the tube−tube interaction could also affect the phonon relaxation, much as the effect of substrate for the phonon relaxation in monolayer graphene.[23]

In summary, we demonstrated the first measurement on ultrafast phonon dynamics in individual chirality-resolved SWNTs. Our results revealed that the phonon lifetime in different species, metallic or semiconducting, is different and relates to their unique electronic structures. With the recent advances on the growth of chirality-controlled metallic and semiconducting SWNTs,[38] the realization of 5 nm gate lengths in individual semiconducting SWNT field-effect transistors,[39] and the achievement of an overall device footprint of 40 nm in an extremely scaled individual semiconducting carbon nanotube transistor,[40] our study can be useful for optimizing the design of SWNT electronic/photonic devices with better understanding of the energy dissipation in SWNTs.

■ ASSOCIATED CONTENT

Supporting Information

The Supporting Information is available free of charge on the ACS Publications website at DOI: 10.1021/acs.nanolett.8b00341.

Sample preparation and characterization; technical details of experimental measurement and data analysis; detailed information for 14 SWNTs studied (PDF)

■ AUTHOR INFORMATION

Corresponding Authors

*E-mail: swwu@fudan.edu.cn.
*E-mail: khliu@pku.edu.cn.

ORCID

Wei-Tao Liu: 0000-0003-0566-671X
Kaihui Liu: 0000-0002-8781-2495
Shiwei Wu: 0000-0001-9838-9066

Author Contributions

T.J. and H.H. contributed equally to this work.

Notes

The authors declare no competing financial interest.

■ ACKNOWLEDGMENTS

This work was supported by the National Basic Research Program of China (2014CB921601 and 2016YFA0300903, 2016YFA0301002), the National Natural Science Foundation of China (91421108, 11474006, and 51522201), the Science and Technology Commission of Shanghai Municipality (16JC1400401), and the Shu Guang Project (Grant No. 11SG05).

■ REFERENCES

(1) Iijima, S. *Nature* **1991**, *354*, 56−58.
(2) Spataru, C. D.; Ismail-Beigi, S.; Benedict, L. X.; Louie, S. G. *Phys. Rev. Lett.* **2004**, *92*, 077402.
(3) Leroy, B. J.; Lemay, S. G.; Kong, J.; Dekker, C. *Nature* **2004**, *432*, 371−374.
(4) Plentz, F.; Ribeiro, H. B.; Jorio, A.; Strano, M. S.; Pimenta, M. A. *Phys. Rev. Lett.* **2005**, *95*, 247401.
(5) Wu, Y.; Maultzsch, J.; Knoesel, E.; Chandra, B.; Huang, M.; Sfeir, M. Y.; Brus, L. E.; Hone, J.; Heinz, T. F. *Phys. Rev. Lett.* **2007**, *99*, 027402.
(6) Yao, Z.; Kane, C. L.; Dekker, C. *Phys. Rev. Lett.* **2000**, *84*, 2941−2944.
(7) Javey, A.; Guo, J.; Paulsson, M.; Wang, Q.; Mann, D.; Lundstrom, M.; Dai, H. J. *Phys. Rev. Lett.* **2004**, *92*, 106804.
(8) Lazzeri, M.; Piscanec, S.; Mauri, F.; Ferrari, A. C.; Robertson, J. *Phys. Rev. Lett.* **2005**, *95*, 236802.
(9) Pop, E.; Mann, D.; Cao, J.; Wang, Q.; Goodson, K. E.; Dai, H. J. *Phys. Rev. Lett.* **2005**, *95*, 155505.
(10) Lazzeri, M.; Mauri, F. *Phys. Rev. B: Condens. Matter Mater. Phys.* **2006**, *73*, 165419.
(11) Song, D.; Wang, F.; Dukovic, G.; Zheng, M.; Semke, E. D.; Brus, L. E.; Heinz, T. F. *Phys. Rev. Lett.* **2008**, *100*, 225503.

DOI: 10.1021/acs.nanolett.8b00341
Nano Lett. 2018, 18, 2590−2594

(12) Chatzakis, I.; Yan, H.; Song, D.; Berciaud, S.; Heinz, T. F. *Phys. Rev. B: Condens. Matter Mater. Phys.* **2011**, *83*, 205411.
(13) Jorio, A.; Fantini, C.; Dantas, M.; Pimenta, M. A.; Souza Filho, A. G.; Samsonidze, G. G.; Brar, V. W.; Dresselhaus, G.; Dresselhaus, M. S.; Swan, A. K.; Unlu, M. S.; Goldberg, B. B.; Saito, R. *Phys. Rev. B: Condens. Matter Mater. Phys.* **2002**, *66*, 115411.
(14) Lazzeri, M.; Piscanec, S.; Mauri, F.; Ferrari, A. C.; Robertson, J. *Phys. Rev. B: Condens. Matter Mater. Phys.* **2006**, *73*, 155426.
(15) Shah, J. *Ultrafast Spectroscopy of Semiconductors and Semiconductor Nanostructures*; Springer: Berlin, 1996.
(16) Myllyperkio, P.; Herranen, O.; Rintala, J.; Jiang, H.; Mudimela, P. R.; Zhu, Z.; Nasibulin, A. G.; Johansson, A.; Kauppinen, E. I.; Ahlskog, M.; Pettersson, M. *ACS Nano* **2010**, *4*, 6780−6786.
(17) Gao, B.; Hartland, G. V.; Huang, L. B. *ACS Nano* **2012**, *6*, 5083−5090.
(18) Gao, B.; Hartland, G. V.; Huang, L. B. *J. Phys. Chem. Lett.* **2013**, *4*, 3050−3055.
(19) Kang, K.; Ozel, T.; Cahill, D. G.; Shim, M. *Nano Lett.* **2008**, *8*, 4642−4647.
(20) Ikeda, K.; Uosaki, K. *Nano Lett.* **2009**, *9*, 1378−1381.
(21) Yan, H.; Song, D.; Mak, K. F.; Chatzakis, I.; Maultzsch, J.; Heinz, T. F. *Phys. Rev. B: Condens. Matter Mater. Phys.* **2009**, *80*, 121403.
(22) Kang, K.; Abdula, D.; Cahill, D. G.; Shim, M. *Phys. Rev. B: Condens. Matter Mater. Phys.* **2010**, *81*, 165405.
(23) Wu, S. W.; Liu, W.-T.; Liang, X. G.; Schuck, P. J.; Wang, F.; Shen, Y. R.; Salmeron, M. *Nano Lett.* **2012**, *12*, 5495−5499.
(24) Wang, Z. L.; Poncharal, P.; de Heer, W. A. *J. Phys. Chem. Solids* **2000**, *61*, 1025−1030.
(25) Liu, Z. J.; Qin, L. C. *Chem. Phys. Lett.* **2005**, *408*, 75−79.
(26) Liu, K. H.; Xu, Z.; Wang, W. L.; Gao, P.; Fu, W. Y.; Bai, X. D.; Wang, E. G. *J. Phys. D: Appl. Phys.* **2009**, *42*, 125412.
(27) Sfeir, M. Y.; Wang, F.; Huang, L. M.; Chuang, C. C.; Hone, J.; O'Brien, S. P.; Heinz, T. F.; Brus, L. E. *Science* **2004**, *306*, 1540−1543.
(28) Liu, K. H.; Deslippe, J.; Xiao, F.; Capaz, R. B.; Hong, X.; Aloni, S.; Zettl, A.; Wang, W.; Bai, X. D.; Louie, S. G.; Wang, E. G.; Wang, F. *Nat. Nanotechnol.* **2012**, *7*, 325−329.
(29) Liu, K. H.; Jin, C. H.; Hong, X. P.; Kim, J.; Zettl, A.; Wang, E. G.; Wang, F. *Nat. Phys.* **2014**, *10*, 737−742.
(30) Liu, K. H.; Hong, X. P.; Choi, S.; Jin, C.; Capaz, R. B.; Kim, J.; Wang, W.; Bai, X.; Louie, S. G.; Wang, E. G.; Wang, F. *Proc. Natl. Acad. Sci. U. S. A.* **2014**, *111*, 7564−7569.
(31) Saito, R.; Dresselhaus, G.; Dresselhaus, M. S. *Physical Properties of Carbon Nanotubes*; Imperial College Press: London, 1998.
(32) Gambetta, A.; Manzoni, C.; Menna, E.; Meneghetti, M.; Cerullo, G.; Lanzani, G.; Tretiak, S.; Piryatinski, A.; Saxena, A.; Martin, R. L.; Bishop, A. R. *Nat. Phys.* **2006**, *2*, 515−520.
(33) Htoon, H.; O'Connell, M. J.; Doorn, S. K.; Klimov, V. I. *Phys. Rev. Lett.* **2005**, *94*, 127403.
(34) Perebeinos, V.; Tersoff, J.; Avouris, P. *Phys. Rev. Lett.* **2005**, *94*, 027402.
(35) Wang, F.; Dukovic, G.; Brus, L. E.; Heinz, T. F. *Science* **2005**, *308*, 838−841.
(36) Wang, F.; Cho, D. J.; Kessler, B.; Deslippe, J.; Schuck, P. J.; Louie, S. G.; Zettl, A.; Heinz, T. F.; Shen, Y. R. *Phys. Rev. Lett.* **2007**, *99*, 227401.
(37) Yan, J.; Zhang, Y.; Kim, P.; Pinczuk, A. *Phys. Rev. Lett.* **2007**, *98*, 166802.
(38) Zhang, S.; Kang, L.; Wang, X.; Tong, L.; Yang, L.; Wang, Z.; Qi, K.; Deng, S.; Li, Q.; Bai, X.; Ding, F.; Zhang, J. *Nature* **2017**, *543*, 234−238.
(39) Qiu, C.; Zhang, Z.; Xiao, M.; Yang, Y.; Zhong, D.; Peng, L.-M. *Science* **2017**, *355*, 271−276.
(40) Cao, Q.; Tersoff, J.; Farmer, D. B.; Zhu, Y.; Han, S.-J. *Science* **2017**, *356*, 1369.

DOI: 10.1021/acs.nanolett.8b00341
Nano Lett. 2018, 18, 2590−2594